Plasmon-Fano Resonance inside the Particle-Hole Excitation Spectrum of Simple Metals and Semiconductors

K. Sturm

Institut für Festkörperforschung, Forschungszentrum Jülich GmbH, D-5170 Jülich, Federal Republic of Germany

W. Schülke and J. R. Schmitz

Institut für Physik, Universität Dortmund, D-4600 Dortmund 50, Federal Republic of Germany

(Received 9 August 1991)

It is shown that local-field effects in simple metals and semiconductors couple the plasmon into the large-wave-vector **q** particle-hole excitation spectrum, leading to a plasmon antiresonance (plasmon-Fano resonance). The resulting structure is observed in inelastic x-ray scattering spectroscopy (IXSS) of single-crystal Si for scattering vectors **q** along the ⟨111⟩ direction. The inclusion of exchange and correlation effects is important to obtain good agreement between theory and experiment. Previously unexplained structures in the IXSS of single-crystal Li for **q** along the ⟨110⟩ direction and of single-crystal Be for **q** along ⟨100⟩ and ⟨001⟩ are also identified as plasmon-Fano resonances.

PACS numbers: 71.45.Gm

Structures in the excitation spectra of nearly-free-electron (NFE) systems, such as simple metals and *sp*-band semiconductors with wave vectors **q** beyond the plasmon cutoff wave vector, have been of continuing theoretical and experimental interest because of expected exchange and correlation (xc) effects at large **q** (see, for example, Refs. [1–4]). We demonstrate in this Letter that a structure observed in inelastic x-ray scattering spectroscopy (IXSS) of single-crystal Si is caused primarily by dynamical local-field effects due to the inhomogeneity of the system. The agreement with experiment is considerably improved when xc effects are included.

To understand the effect we first consider the jellium model. In the self-consistent-field (SCF) approximation, the excitation spectrum consists of sharp plasmons for q smaller than the plasmon cutoff wave vector q_c, and a broad continuum of particle-hole (p-h) excitations which shift to higher frequency ω with increasing q.

In real systems such as simple metals and *sp*-band semiconductors, the weak effective periodical potential $V(\mathbf{r})=\sum_{\mathbf{G}} V_{\mathbf{G}} e^{i\mathbf{G}\cdot\mathbf{r}}$ couples both types of excitations via umklapp processes involving reciprocal-lattice vectors **G**. The coupling strength depends on the size of the pseudopotential Fourier coefficients $U_{\mathbf{G}}$; $V_{\mathbf{G}}=S_{\mathbf{G}}U_{\mathbf{G}}$, where $S_{\mathbf{G}}$ is the appropriate crystal-structure factor. As a well-known consequence, the plasmon can decay into p-h excitations by interband transitions and by local-field effects, resulting in a characteristic **q**-dependent linewidth and a small **q**-dependent frequency shift [5].

The influence of the plasmon on the large-**q** p-h excitation spectrum due to the coupling by the crystal potential has not been considered previously. Here we report measurements and calculations of the dynamical electronic-structure factor $S(\mathbf{q},\omega)$ for single-crystal Si in the large-**q** regime to investigate this effect.

Simple metals and semiconductors serve as model systems where these effects can be analyzed by simple means, but similar effects are present in more complicated systems such as noble and transition metals.

In recent years the large-**q** excitation spectrum has become accessible to experimental investigations by IXSS, where both experimental details and the evaluation of the data have been described elsewhere [6–8]. Using synchrotron radiation from the DORIS storage ring, monochromatized to 7.99 keV, we have measured $S(\mathbf{q},\omega)$ of Si for **q** along the ⟨100⟩, ⟨110⟩, and ⟨111⟩ directions, with a 1.5-eV energy resolution and a **q** resolution of $\delta q/q=0.1$ for q values between 0.4 and 1.8 a.u. We had about 2000–3000 counts per measured point in the maximum of the energy-loss spectrum. To obtain a complete frequency spectrum took about 10 h.

We found for a q range between 0.8 and 1.8 a.u. a characteristic fine structure in the measured $S(\mathbf{q},\omega)$ spectra for **q** along $\mathbf{G}_{111}$, which is absent in the corresponding measured $S(\mathbf{q},\omega)$ spectra for **q** along the ⟨110⟩ direction [9]. The triangles, for example, in Fig. 1 are experimental results for $q=1.25$ a.u. [Fig. 1(a)] and for $q=1.45$ a.u. [Fig. 1(b)] with **q** in the ⟨111⟩ direction. The relevant fine structure is close to the plasma frequency and is characterized by a relative minimum followed by a steep rise and a relative maximum. The magnitude of the fine structure is apparent from a comparison of the ⟨111⟩ points (triangles) with those for **q** along ⟨110⟩ [circles in Fig. 2(b)] or with those for **q** along ⟨100⟩ [circles in Fig. 2(c)]. Squares in Figs. 2(b) and 2(c) show the difference between the ⟨111⟩ and ⟨110⟩ spectra and the ⟨100⟩ spectrum, respectively.

The theory, as derived below including xc effects [Fig. 2(a) and solid lines in Fig. 1], explains this fine structure as a plasmon antiresonance or plasmon-Fano resonance inside the p-h continuum. The dotted line in Fig. 1(a) is calculated within the random-phase approximation (RPA). We call this a Fano resonance because it arises from the interaction of a discrete excitation (plasmon)

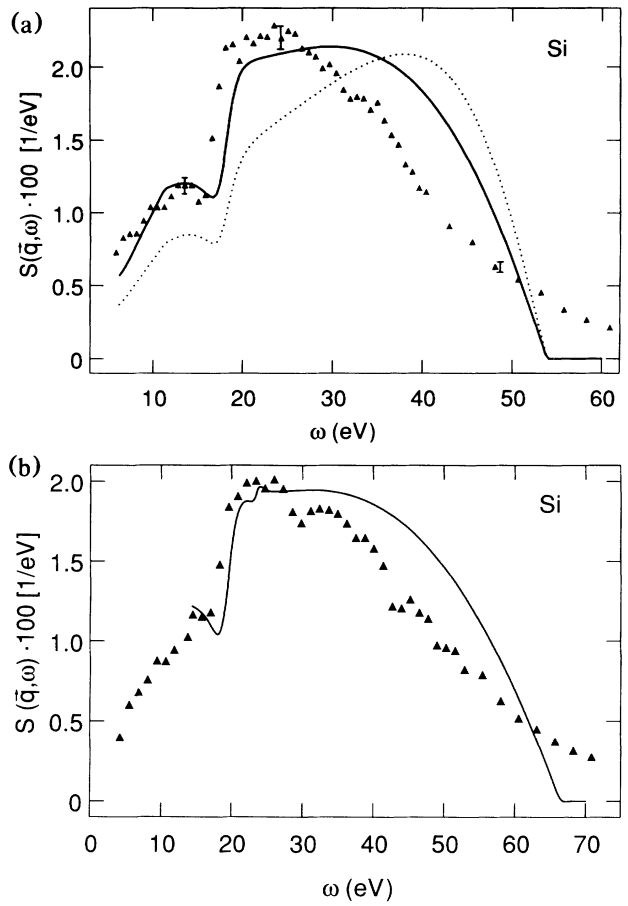

FIG. 1. Dynamic structure factor for single-crystal Si for **q** in the ⟨111⟩ direction as a function of ω: (a) $q=1.25$ a.u.; (b) $q=1.45$ a.u. Triangles, IXSS data; solid lines, theory, Eq. (5), including xc effects; dotted curve, RPA theory.

with an excitation continuum (p-h excitations).

The theory makes use of the fluctuation-dissipation theorem and relates $S(\mathbf{q},\omega)$ to the density-density response function. This response function can be calculated within the SCF approximation from the microscopic dielectric matrix $\tilde{\epsilon}_{\mathbf{GG}'}(\mathbf{k},\omega)$ spanned by reciprocal-lattice vectors. Exchange and correlation effects are included approximately by a local-field factor $G^0(q)$ (not to be confused with local-field effects due to inhomogeneity) of the homogeneous electron gas. We obtain

$$S(\mathbf{q},\omega)=\frac{\hbar q^2}{4\pi^2 e^2 n_0}\,\mathrm{Im}[-\tilde{\epsilon}^{-1}(\mathbf{k},\omega)]_{\mathbf{GG}}\times\left(\frac{1}{1-G^0(|\mathbf{k}+\mathbf{G}|)}\right) \tag{1}$$

Here $[\tilde{\epsilon}^{-1}(\mathbf{k},\omega)]_{\mathbf{GG}}$ is the **GG** element of the inverse of the microscopic dielectric matrix which is defined by

$$\tilde{\epsilon}_{\mathbf{GG}'}(\mathbf{k},\omega)=\delta_{\mathbf{GG}'}-v_{\mathbf{k}+\mathbf{G}}[1-G^0(|\mathbf{k}+\mathbf{G}|)]\times\chi^0(\mathbf{k}+\mathbf{G},\mathbf{k}+\mathbf{G}';\omega); \tag{2}$$

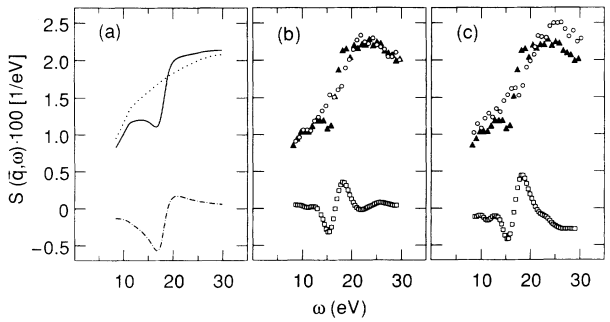

FIG. 2. Dynamic structure factor for single-crystal Si for $q=1.25$ a.u. (a) Theory for **q** along ⟨111⟩: dotted line, p-h spectrum [first term of Eq. (5)]; dash-dotted line, plasmon-Fano resonance [second term of Eq. (5)]; solid line, total spectrum [Eq. (5)]. (b) Experiment: triangles, IXSS data for **q** along ⟨111⟩; circles, IXSS data for **q** along ⟨110⟩; squares, difference between experimental ⟨111⟩ and ⟨110⟩ spectra. (c) Experiment: triangles, IXSS data for **q** along ⟨111⟩; circles, IXSS data for **q** along ⟨100⟩; squares, difference between experimental ⟨111⟩ and ⟨100⟩ spectra.

$v_{\mathbf{k}+\mathbf{G}}=4\pi e^2/|\mathbf{k}+\mathbf{G}|^2$, n_0 is the mean electron density, and $\chi^0(\mathbf{k}+\mathbf{G},\mathbf{k}+\mathbf{G}';\omega)$ is the independent-particle density-density response function. We have used the local-field factor of Utsumi and Ichimaru [10], which satisfies various requirements in the small- and large-**q** limits. If $G^0(q)$ is neglected, $\tilde{\epsilon}_{\mathbf{GG}'}(\mathbf{k},\omega)$ reduces $\epsilon_{\mathbf{GG}'}(\mathbf{k},\omega)$ and the standard RPA [11] is recovered. The reciprocal-lattice vector **G** in Eq. (1) is fixed by the requirement

$$\mathbf{q}=\mathbf{k}+\mathbf{G}, \tag{3}$$

which relates the scattering vector **q** to the crystal momentum **k**, confined to the first Brillouin zone (BZ), and to the required **G**.

To understand the physical effect it is sufficient to calculate $S(\mathbf{q},\omega)$ within a two-plasmon-band model that was previously used to study the occurrence of plasmon bands near the BZ boundary in semiconductors [12]. In this case the dielectric matrix is approximated by an effective 2×2 matrix, which is then evaluated within the NFE approximation. For simplicity we used a local empirical pseudopotential [13] that is known to give, for example, a good description of the plasmon line shape [5].

For small **q**, i.e., $\mathbf{q}=\mathbf{k}$ and $\mathbf{G}=0$, we obtain

$$S(\mathbf{q},\omega)=\frac{\hbar q^2}{4\pi^2 e^2 n_0}\,\mathrm{Im}[-\tilde{\epsilon}^{-1}(\mathbf{k},\omega)]_{00}\frac{1}{1-G^0(k)}\approx\frac{\hbar q^2}{4\pi^2 e^2 n_0}\,\mathrm{Im}\left[-1\Big/\left(\tilde{\epsilon}_{00}-\sum_{\mathbf{G}\neq 0}\tilde{\epsilon}_{0\mathbf{G}}\tilde{\epsilon}_{\mathbf{G}0}/\tilde{\epsilon}_{\mathbf{GG}}\right)\right]\times\frac{1}{1-G^0(k)}, \tag{4}$$

where we have suppressed the arguments **k** and ω in the elements of the dielectric matrix. The diagonal term $\tilde{\epsilon}_{00}$ contains interband transitions, and the nondiagonal ele-

ments provide the coupling to the short-wavelength density fluctuations described by $1/\tilde{\epsilon}_{\mathbf{GG}}$, known as local-field effects. The second line of Eq. (4) yields a proper description of the plasmon line within the one-plasmon-band model [5] to which the two-band model reduces for $\mathbf{q}$ well inside the BZ.

The theoretical curves in Fig. 1 are evaluated from Eq. (1) for $\mathbf{G}=\mathbf{G}_{111}$, and the result obtained from the effective 2×2 matrix can be written in the form

$$S(\mathbf{q},\omega)=\frac{\hbar q^2}{4\pi^2 e^2 n_0}\,\mathrm{Im}\left[\frac{-1}{\tilde{\epsilon}_{\mathbf{GG}}}+\frac{\tilde{\epsilon}_{\mathbf{G}0}\tilde{\epsilon}_{0\mathbf{G}}}{\tilde{\epsilon}^2_{\mathbf{GG}}}[-\tilde{\epsilon}^{-1}(\mathbf{k},\omega)]_{00}\right]\times\frac{1}{1-G^0(|\mathbf{k}+\mathbf{G}|)}\,. \tag{5}$$

Equation (5) provides the key to the understanding of the plasmon-Fano resonance. The first term in the large square brackets accounts for the p-h excitation spectrum; the second term consists of a coupling function $F_{\mathbf{G}}(\mathbf{k},\omega)=\tilde{\epsilon}_{\mathbf{G}0}\tilde{\epsilon}_{0\mathbf{G}}/\tilde{\epsilon}^2_{\mathbf{GG}}$ and a function that, according to Eq. (4), describes the plasmon line. $F_{\mathbf{G}}(\mathbf{k},\omega)$ couples large $\mathbf{q}=\mathbf{k}+\mathbf{G}$ ($\mathbf{G}=\mathbf{G}_{111}$) density fluctuations, i.e., p-h excitations, to small $\mathbf{k}$ density fluctuations, namely, plasmons. If $F_{\mathbf{G}}(\mathbf{k},\omega)$ were real and positive, we would simply have a plasmon peak of weight $F_{\mathbf{G}}(\mathbf{k},\omega_p(\mathbf{k}))$ superimposed on the p-h spectrum. However, $F_{\mathbf{G}}(\mathbf{k},\omega)$ is complex with negative real and imaginary parts. Whereas $\mathrm{Im}[-\tilde{\epsilon}^{-1}(\mathbf{k},\omega)]_{00}$ is always positive, $\mathrm{Re}[-\tilde{\epsilon}^{-1}(\mathbf{k},\omega)]_{00}$ becomes negative for $\omega>\omega_p(\mathbf{k})$. This explains the behavior of the second term of Eq. (5), which is illustrated by the dash-dotted curve in Fig. 2(a). As a consequence, the coupled plasmon appears as an antiresonance with some resonance behavior on the high-frequency side typical of a Fano resonance. When added to the p-h spectrum [dotted curve in Fig. 2(a)], the resulting curve (solid line) exhibits the structure that is observed experimentally [see Fig. 1(a)]. The Fano resonance experimentally observed for $q=1.45$ a.u. is in similar agreement with the present theory. Again a steep flank close to the plasma frequency $\omega_p(\mathbf{k})$ characterizes the $S(\mathbf{q},\omega)$ spectrum. The low-frequency part of the spectrum could not be calculated because the lower limit of validity of the perturbation theory increases with increasing $\mathbf{k}$. (Details will be published elsewhere.)

Within the two-plasmon-band model we have also calculated $S(\mathbf{q},\omega)$ from Eq. (5) for $\mathbf{q}$ along $\langle 110\rangle$ with $\mathbf{G}=\mathbf{G}_{220}$ and for $\mathbf{q}$ along $\langle 100\rangle$ with $\mathbf{G}=\mathbf{G}_{200}$. The resulting curve for $\mathbf{q}$ along $\langle 110\rangle$ exhibits an extremely faint antiresonance near the plasma frequency and is thus almost identical to the p-h curve [dotted line in Fig. 2(a)]. For $\mathbf{q}$ along $\langle 100\rangle$ the antiresonance is completely absent because $V_{\mathbf{G}_{200}}$ vanishes. This is the justification for the comparison of the calculated Fano resonance [second term of Eq. (5)] with the difference (squares) of the experimental $\langle 111\rangle$ (triangles) spectrum and the $\langle 110\rangle$ and $\langle 100\rangle$ (circles) spectra in Figs. 2(b) and 2(c). The squares are derived using a cubic spline interpolation of the experimental spectra.

We have also evaluated the dynamical structure factor for Al and for Li in the large-$\mathbf{q}$ regime. In Al, the pseudopotential is very small, leading to a narrow plasmon line and a rather small coupling function $F_{\mathbf{G}}(\mathbf{k},\omega)$. Hence it is presently difficult to observe the Fano resonance in Al with the energy resolution attainable in IXSS. Li is a better candidate, because it exhibits a broad plasmon line like Si. Indeed, earlier IXSS spectra [7] of Li (see Fig. 13 of Ref. [7]) exhibit structure in the relevant $(\mathbf{q},\omega)$ regime for $\mathbf{q}$ in the $\langle 110\rangle$ direction. Clear indications of Fano-like structures at frequencies near the plasmon frequency are also present in earlier IXSS spectra of Be, mainly for $\mathbf{q}$ in the $\langle 100\rangle$ and $\langle 001\rangle$ directions within a q range between 1.0 and 1.4 a.u. (see Fig. 2 of Ref. [8]).

The identification of this plasmon antiresonance is essential in the discussion of the xc effects expected to be particularly important for large $\mathbf{q}$. As is demonstrated in Fig. 1, the inclusion of xc effects improves the agreement with experiment considerably, but they do not themselves produce the structure, as has been suggested in the past [3,4].

Finally we note some limitations of the present theory. Although the plasmon-Fano resonance is properly reproduced, there is still some discrepancy between theory and experiment on the high-energy side. The inclusion of xc effects via a static local-field factor [10] causes a considerable redistribution of oscillator strength from the high- to the low-frequency side of the p-h spectrum, but not enough to give complete agreement with the experiment. Note that no adjustable parameter has been used in the calculation.

Furthermore, the p-h spectrum [first term in Eq. (5)] has been evaluated in the free-electron approximation, which contributes to the lack of fine structure in the theoretical curves. This is not important to understand the effect considered in this Letter, because the coupling function $F_{\mathbf{G}}(\mathbf{k},\omega)$ is of order $|V_{\mathbf{G}}|^2$, whereas $[-\tilde{\epsilon}^{-1}(\mathbf{k},\omega)]_{00}$ is of order $1/|V_{\mathbf{G}}|^2$ close to the resonance. For ω decreasing towards the energy gap, perturbation theory becomes increasingly inaccurate and finally breaks down. Thus the theoretical curves have been calculated only for $\omega\gtrsim 6$ eV.

We have shown that, even in NFE systems such as simple metals and semiconductors, the weak effective crystal potential can give rise to considerable structure in the large-$(\mathbf{q},\omega)$ p-h spectrum, due to the coupling of a resonant mode. Although the crystal potential is of primary importance for the existence of the plasmon-Fano resonance, the inclusion of xc effects is essential for a quantitative understanding of the spectra.

We thank A. Kaprolat and H. Schulte-Schrepping for valuable help with measurements at DORIS/HASYLAB (Hamburger Synchrotronstrahlungslabor). The measurements have been supported by the German Federal Ministry of Research and Technology under Contract No. 05

434 AXB. We are grateful to R. O. Jones for a critical reading of the manuscript.

[1] P. M. Platzman and P. Eisenberger, Phys. Rev. Lett. **33**, 152 (1974).
[2] C. H. Chen, A. E. Meixner, and B. M. Kincaid, Phys. Rev. Lett. **44**, 951 (1980).
[3] F. Green, D. N. Lowy, and J. Szymański, Phys. Rev. Lett. **48**, 638 (1982).
[4] F. Green, D. Neilson, and J. Szymański, Phys. Rev. B **31**, 2796 (1985).
[5] K. Sturm and L. E. Oliveira, Phys. Rev. B **22**, 6268 (1980).
[6] W. Schülke and H. Nagasawa, Nucl. Instrum. Methods **222**, 203 (1984).
[7] W. Schülke, H. Nagasawa, S. Mourikis, and P. Lanzki, Phys. Rev. B **33**, 6744 (1986).
[8] W. Schülke, H. Nagasawa, S. Mourikis, and A. Kaprolat, Phys. Rev. B **40**, 12215 (1989).
[9] For details, see J. R. Schmitz, Ph.D. thesis, University of Dortmund, 1991 (unpublished).
[10] K. Utsumi and S. Ichimaru, Phys. Rev. A **26**, 603 (1982).
[11] N. Wiser, Phys. Rev. **129**, 62 (1963).
[12] L. E. Oliveira and K. Sturm, Phys. Rev. B **22**, 6283 (1980).
[13] J. R. Chelikowsky and M. L. Cohen, Phys. Rev. B **10**, 5095 (1974).